Chapter 6

Numerical Simulation of Residual Stresses in Welding and Ultrasonic Impact Treatment Process

Lanqing Tang, Ayhan Ince and Jing Zheng

Additional information is available at the end of the chapter

http://dx.doi.org/10.5772/intechopen.72394

Abstract

Welding technology is considered as a reliable and efficient joining method, which has been widely used in almost all the industry departments. Detrimental factors induced by welding such as micro-cracks/flaws, tensile residual stresses, high stress concentration may degrade the mechanical and fatigue properties of weld joints. Ultrasonic impact treatment (UIT) is considered one of the most efficient post-weld treatment which could improve the fatigue performance of weld joints. In this study, the effect of the UIT on residual stress distribution of 304L weld joints was particularly investigated. FE analysis simulation and the XRD experiment were performed to predict and measure residual stresses of both as-welded and the UIT-treated joints. Compared results show that simulated stresses are in good agreement with the experimental results along various paths, confirming the validity of welding model. The UIT introduces a compressive residual stress layer with depth between 2 and 3 mm near the impacting surface of weld joint.

Keywords: ultrasonic impact treatment (UIT), finite element modeling (FEM), weld residual stress, stress and strain, weld simulation

1. Introduction

Welding technology has been widely applied in the fields of automobile, aviation, nuclear, vessel manufacturing and other industrial sectors due to its low cost, geometrical flexibility and desirable mechanical properties [1]. On the other hand, welding comes with the expense of some detrimental effects on welded structures such as micro-cracks/flaws, high stress concentration and tensile residual stresses. Hence, from the point view of fatigue design, welded areas are deemed as weak structural joints where cracks and tensile residual stresses are easily to be found [2]. A number of numerical techniques have been developed to model the

influence of tensile residual stresses on fatigue strength of welded joints [3–6]. Over the past several decades, numerous post-weld treatment techniques, including grinding, TIG dressing, hammer peening and shot peening, have been developed to address this vexing issue and improve fatigue performance of weld joints [7]. These treatments are generally classified into two different categories: geometry improvement and residual stress modification techniques. Geometry improvement techniques such as TIG dressing and grinding focus on eliminating flaws and reducing stress concentration of welded components. While residual stress modification techniques like hammer peening and shot peening lay emphasis on introducing beneficial compressive residual stresses and improving residual stress distributions of welded joints [8].

Ultrasonic impact treatment (UIT) is a recently introduced treatment technique developed by Statnikov et al. in former Soviet Union [9]. This technique has become increasingly popular for several reasons such as reducing manpower requirements, eliminating the weld induced distortions. The UIT uses needles or hammer-like rods to impact the welding surface/toe at a high ultrasonic frequency of 18,000–27,000 Hz. The UIT, not only reduces the local stress concentration by modifying the weld toe geometry but also introduces compressive residual stresses by eliminating tensile residual stresses and introducing beneficial compressive stresses [10].

In recent years, numerous studies have been carried out to investigate effects of the UIT on the weld residual stresses and fatigue performance of weld joints [11–14]. A number of numerical models have been developed to predict the residual stress distribution and fatigue performance of UIT-treated weld joints [13, 15]. Meanwhile, experimental studies of the UIT have been also conducted [11, 12, 14]. Various measurement techniques such as X-ray diffraction and neutron diffraction were used to obtain experimental data for the validation of simulated residual stresses. In most of the cases, it has been found that the UIT introduces compressive residual stresses along varying depths and improves fatigue performances of weld joints in various extent. Turski et al. [11] found that the UIT produced compressive residual stress fields of about 2 mm in depth for 304 stainless steel. Liu et al. [12] measured residual stresses of UIT-treated high strength steel weld joints. The results indicated that the UIT had the same effect on both longitudinal and transverse stresses and introduced a compressive residual stress layer up to 4 mm in depth. Foehrenbach et al. [13] developed a computationally efficient approach to predict residual stresses induced by the UIT process using a commercial finite element software package. It was found that compressive residual stresses up to a base material yield strength occurred after the UIT treatment. Dekhtyar et al. [14] studied the effect of the UIT on fatigue behavior of Ti–6Al–4V specimens. Based on experimental data, it was reported that the UIT introduced compressive stresses of −570 MPa, achieving two thirds of yield limit of the material. Fatigue strength of as-welded joints increased by 60% at 10^7 cycles and fatigue life was extended 10^2 times at stress amplitude of 300 MPa.

To assess fatigue life improvement by the UIT treatment, it is necessary to accurately estimate residual stress distribution through finite element analysis (FEA). Recent numerical studies emphasized on the influence of mesh type, material properties, boundary conditions, pin tool size, modeling strategy and material hardening rules on computed numerical results

http://dx.doi.org/10.5772/intechopen.72394

[13, 15, 16]. It was well known that the isotropic hardening model is valid for monotonic loading [9]. However, due to the Bauschinger effect, isotropic hardening model is not suitable for cyclic loadings experienced under of the UIT process [17]. On the other hand, linear kinematic hardening model could be adopted to describe material deformation behavior under cyclic loading conditions, but it could provide reasonable results under small strains loading conditions [18]. Therefore, the combined isotropic-kinematic hardening model, or Chaboche model was applied to the UIT simulation [19, 20]. In addition, in the modeling of the UIT process, regardless the complex components and ultrasonic transducer of the UIT device, the pin impact can be simplified as the movement of the impact pin tool given proper controlling parameters. These parameters consist of impact velocity, the contact force and the pin displacement. Hence, modeling strategies of the UIT can be classified into three categories: velocity-controlled simulation (VCS), force-controlled-simulation (FCS) and displacement-controlled-simulation (DCS) [21–23]. In the VSC strategy, the velocity of the impact pin can be obtained through the approximated motion using a sinusoidal harmonic function, where the first derivative represents the velocity [17]. The FCS strategy defines the pin impact with a given load force while the DCS utilizes the permanent indentation obtained by the UIT to define the displacement of the pin [22, 23].

This paper focuses on effects of the UIT on residual stresses of 304L weld joints. FE analysis was carried out to simulate residual stress distributions of as-welded and the UIT-treated joints. The UIT process was simulated with the pre-existing validated stress field of residual stresses, which considered the effects of the UIT in transverse, longitudinal and through-thickness directions. In addition, the DCS and Chaboche model was introduced to improve both the time efficiency and the preciseness of prediction.

2. Finite element (FE) modeling

2.1. FE modeling of weld joints

FE simulation of both butt and T weld joints have been performed using the Coupled Temperature-Displacement analysis provided by ABAQUS software package. The 3-D finite element models of butt joint and T-joint are depicted in **Figure 1**. As shown in **Figure 2**, to reduce the computation time, the FE models of welded joints were reduced by one-half and one-quarter using the overall symmetry and both models were simplified as the single pass welding. Geometries of both butt and T weld joints were modeled with the C3D8T element. In order to improve computed results, the refined meshes with the minimum element size of 1 × 1 × 1 mm were created in the heat affected zone (HAZ) and the weld area of FE models. The butt joint had 251,585 nodes while the T-joint had 240,692 nodes. Outer surfaces of weld joints were under both radiation and convection condition with emissivity of 0.85 and filming coefficient of 10 W/(m^2°C). As shown in **Figure 2(a)**, for the butt joint, nodes on symmetry plane Y-Z, line H-I/G-J and line G-H were constrained in X-direction, Y-direction and Z-direction, respectively. For the T-joint, similarly, nodes on symmetry plane Y-Z, line F-I/G-H and line F-G were restricted in X axis, Y axis and Z axis, respectively. As seen in

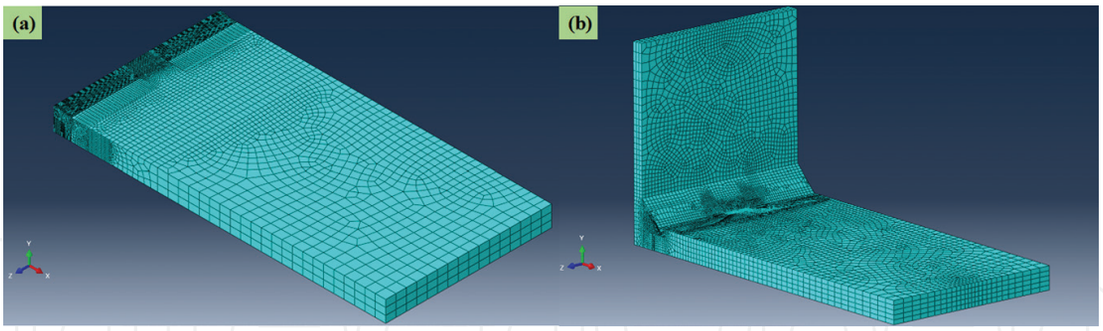

Figure 1. 3-D finite element model: (a) butt joint and (b) T-joint.

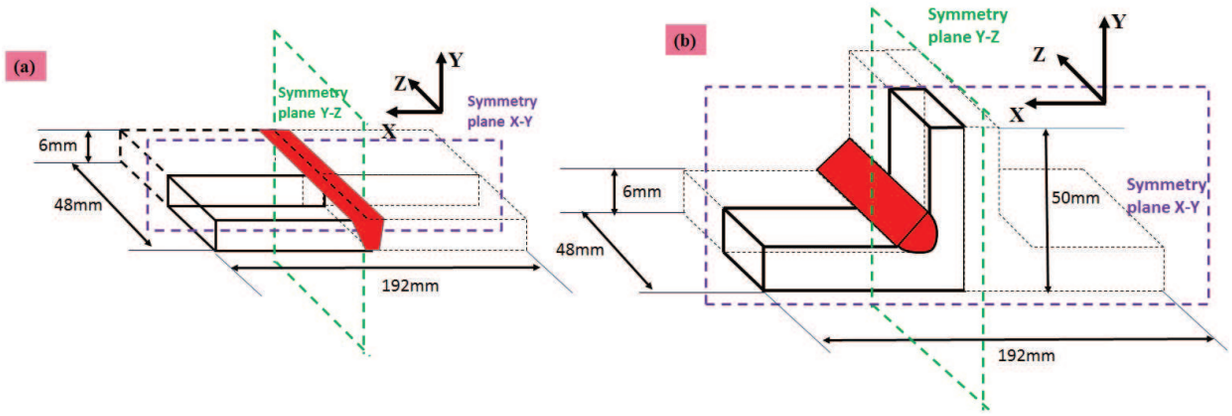

Figure 2. A schematic representation of weld geometry: (a) butt joint and (b) T-joint.

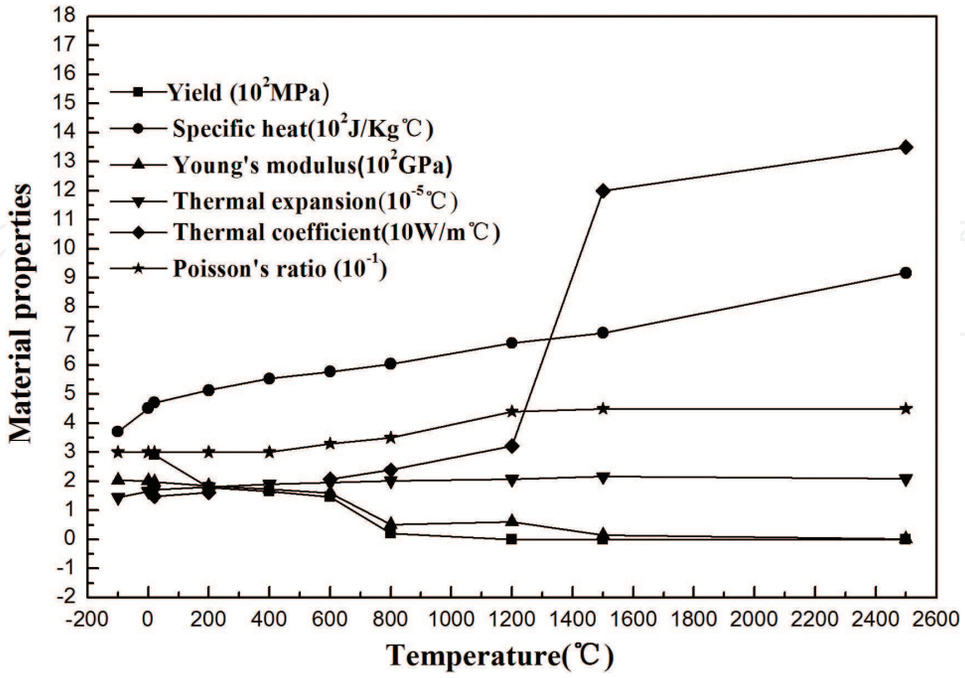

Figure 3. Thermal properties and mechanical properties.

Material	C	Si	Mn	Cr	Ni	S	P	Fe
Base metal (06Cr19Ni10)	0.045	0.45	1.10	17.1	8.00	0.001	0.028	Rest
Electrode (ER308L)	0.03	0.60	1.80	20.0	10.0	0.008	0.015	Rest

Table 1. Chemical composition of base metal and welding electrode (wt%).

Figure 3, temperature dependent properties of 304L were obtained from the literature [24]. A double-ellipsoid heat source model was adopted in numerical simulation of welding process. The actual welding experimental data for welding process and parameters was listed in **Tables 1** and **2**.

2.2. FE modeling of UIT process

In the FE modeling of the UIT process, residual stress results obtained from the welding process were taken as the initial model state. As shown in **Figure 4**, in the middle of the weld zone, an impact area with the minimum element size of 0.1 × 0.1 × 0.5 mm were created in the weld simulation to achieve refined mesh area for the impact simulation so that a re-meshing routine could be avoided to reduce computational time during the UIT simulation. For the material hardening rule, the combined isotropic and kinematic model was used to characterize the material deformation behavior in the FE model of the UIT simulation. The DCS strategy was adopted to control the displacement motion of the pin tool. The pin was set to hit the weld toe at the speed of 2 m/s until it reached the design depth, which was considered as one complete impact. **Figure 5** shows the position and indentation of pin tool for both the butt and T joints. The diameter and the permanent indentation of the pin were 3 and 0.1 mm respectively. The angles of pins in butt joint and T-joint were determined as 75 and 67.5°, respectively. The pin model was modeled as a discrete rigid body and, the pin was traveling along the welding direction and hitting the weld joint every 0.3 mm to ensure a sufficient overlap during the UIT treatment. It was worth noting that in the DCS strategy, the speed of the UIT treatment was considered to be non-essential.

Parameter name	Value
Welding voltage (volts)	24.5
Welding current (amperes)	217
Welding speed (cm/min)	40
Electrode type	ER308L
Welding electrode diameter (mm)	1.2
Shielding gas type	Argon (97%), O_2 (3%)
Shielding gas flow rate (L/min)	20

Table 2. Welding parameters of MIG welding technology.

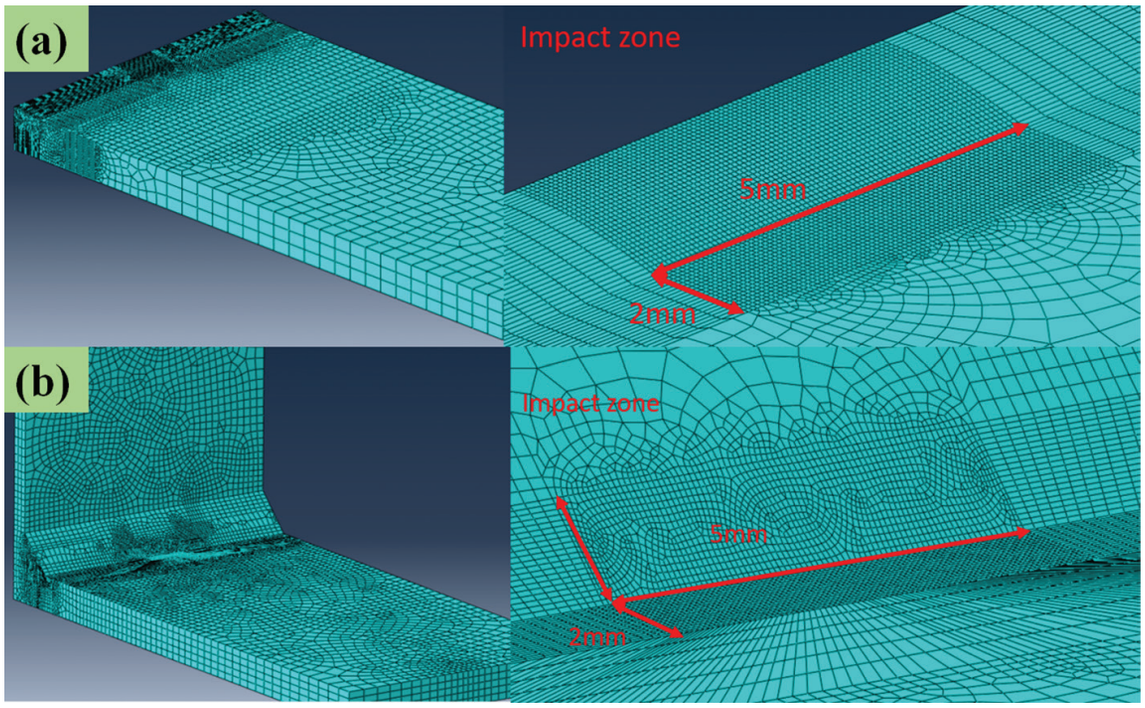

Figure 4. Impact zone of UIT simulation: (a) butt joint and (b) T-joint.

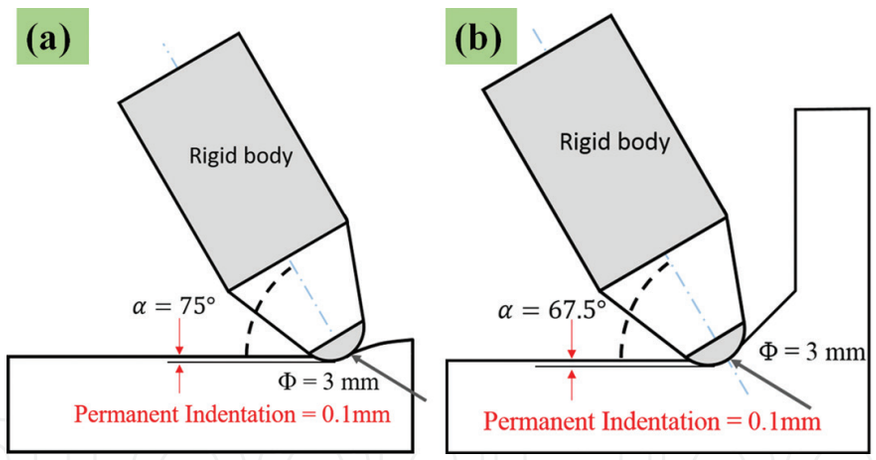

Figure 5. Pin tool position and indentation: (a) butt joint and (b) T-joint.

3. Discussions and results

As shown in **Figures 6–11**, paths A-B, A-C and A-D were selected to evaluate residual stress distributions for the both butt and T joints. Meanwhile, in order to describe residual stresses in directions of X, Y and Z axes, three specific words "transverse," "through-thickness" and "longitudinal" were introduced. The transverse residual stress, the through-thickness residual stress and the longitudinal residual stress indicated σ_xx, σ_yy and σ_zz, respectively.

http://dx.doi.org/10.5772/intechopen.72394

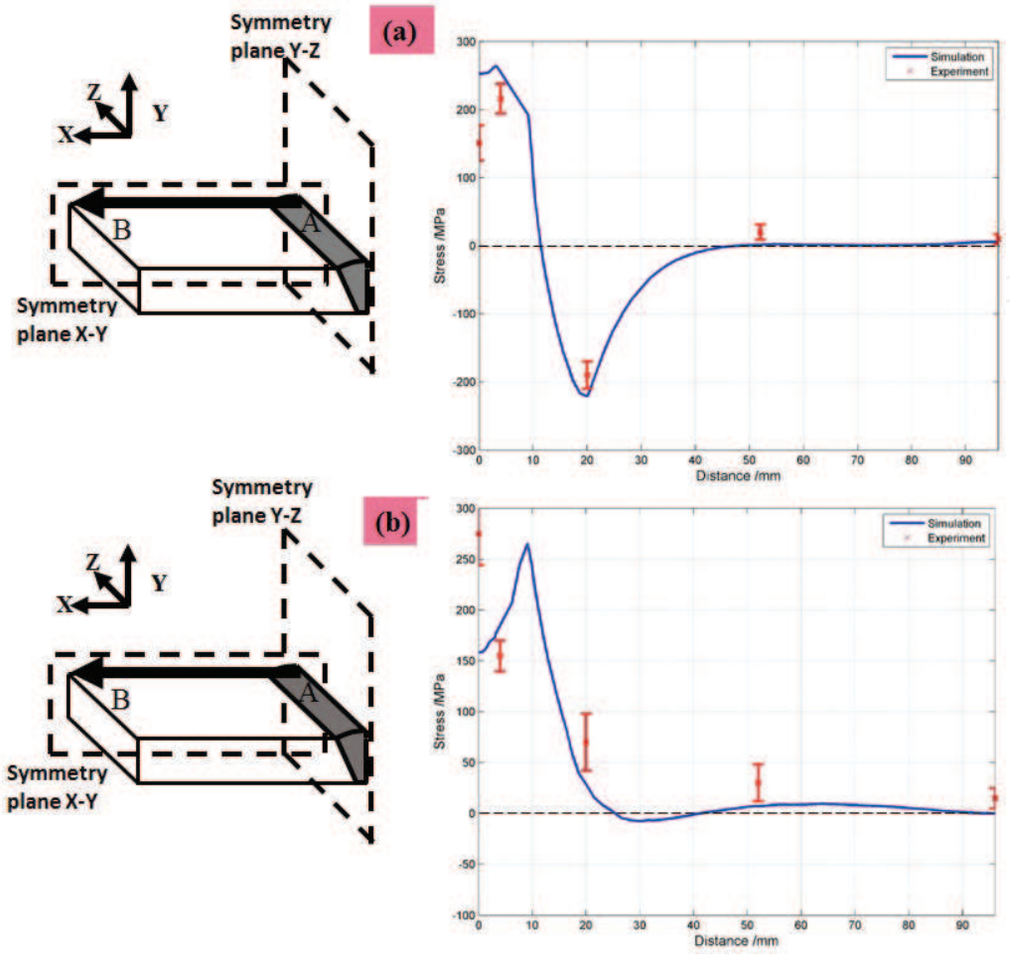

Figure 6. Transverse (a) and longitudinal (b) residual stress distributions along A-B path in butt welded joints.

3.1. Residual stress predictions in weld butt joint

For validating the FE model of welding process, experimental data obtained from previous works [25, 26] were compared with the predicted residual stress results. As shown in **Figures 6** and **7**, predicted and experimental residual stresses of butt joint along paths A-B and A-C are compared, respectively. In particular, the blue lines and the red dots marked in figures demonstrate the predicted residual stresses by FEA and the experimental data obtained by the XRD method, respectively. As depicted in **Figure 6**, both σ_xx and σ_zz reached their maximum values near the weld zone, then dropped as distance from the point A increased and finally stabilized around the zero value. Additionally, it was found that the simulation results are in good agreement with the experimental results along the A-B path, confirming the prediction capability of welding model.

Figure 7 shows the predicted and measured transverse residual stresses along the A-C path. Obviously, at the point A, the point C and in their vicinity, the residual stresses are compressive stresses. In the middle of the A-C path, the transverse residual stresses converted into tensile stresses with peak value of 275 MPa. It was also indicated that there existed some

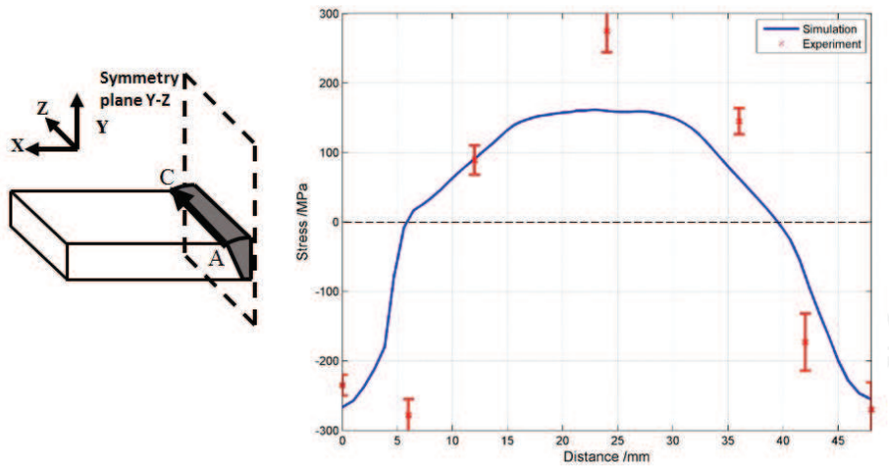

Figure 7. Transverse residual stress distributions along A-C path in butt welded joints.

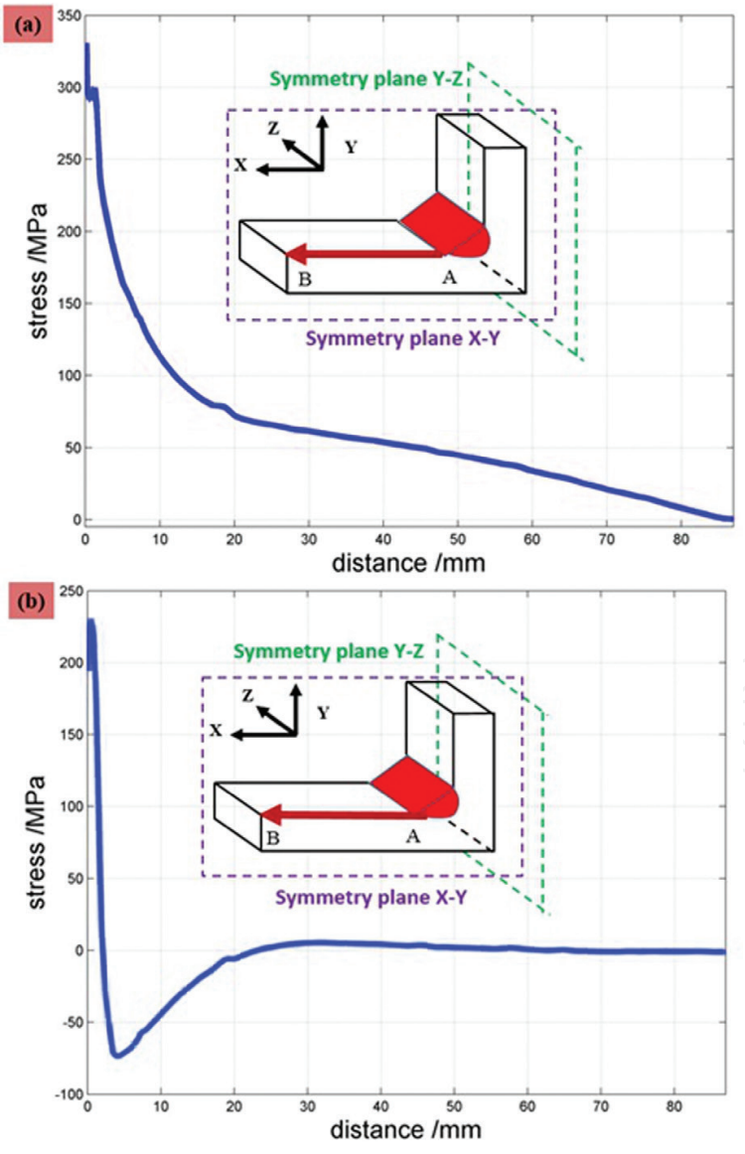

Figure 8. Transverse (a) and longitudinal (b) residual stress distributions along A-B path in T-joints.

http://dx.doi.org/10.5772/intechopen.72394

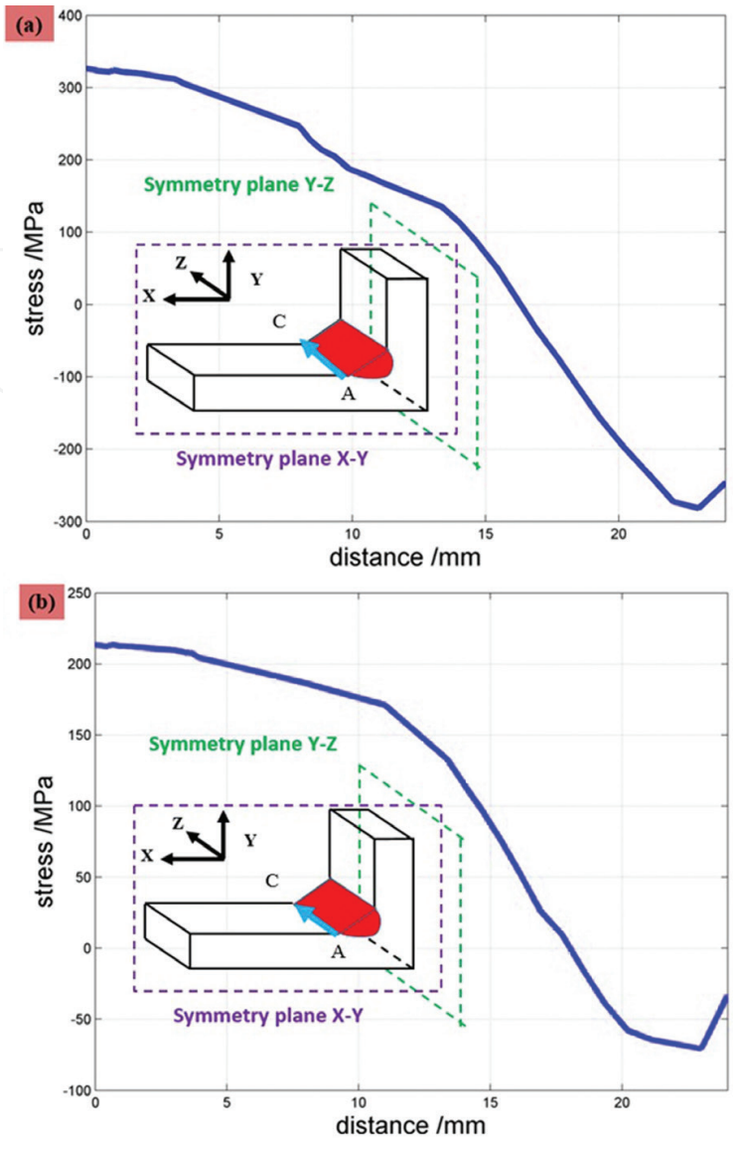

Figure 9. Transverse (a) and longitudinal (b) residual stress distributions along A-C path in T-joints.

errors between the calculated results and the measured ones. The measured residual stresses were higher in the middle of the A-C path but lower at each end of the A-C path. Those errors may be attributed to the measurement error of the XRD method, which was sensitive to the microstructure evolution of welding zone [10].

3.2. Residual stress predictions in weld T-joint

Figures 8 and **9** depict residual stresses of T-joint along the path A-B and path A-C, respectively. As shown in **Figure 8**, along the path A-B, both the transverse residual stress σ_xx and the longitudinal residual stress σ_zz achieved their peaks in the vicinity of weld area. Nevertheless, with the distance from the point A, transverse residual stresses showed a relatively different trend with the longitudinal residual stresses. Transverse residual stresses decreased as the distance from the point A increased and dropped to the zero value at the point B, shown in **Figure 8(a)**. Unlike the transverse residual stresses, longitudinal residual

stresses first dropped dramatically with the increasing distance from the point A and reached the compressive peak value of −75 MPa at the distance of approximately 5 mm from the point A. Then longitudinal residual stresses increase significantly to zero at the distance of 25 mm from the point and remained stable. Notably, both transverse and longitudinal residual stresses changed into negligible values in the relatively far distant from the weld zone, which was consistent with the results of previous studies [27, 29–31, 34, 35].

Figure 9(a) and **(b)** demonstrate transverse and longitudinal residual stresses along the A-C path of the T-joint, respectively. Obviously, the distribution trend of the transverse residual stresses was in line with that of the longitudinal residual stresses. Both the transverse and longitudinal residual stresses obtained their peak values of 345 and 205 MPa in the middle of the welding line (near point A). With the increasing distance from the point A, transverse and longitudinal stresses dropped, changing from the tensile values into the compressive ones. The maximum compressive value of transverse residual stresses (−285 MPa) were considerably higher than that of longitudinal residual stresses (−70 MPa).

3.3. Effects of UIT on weld residual stresses

In order to evaluate the effects of the UIT on residual stresses along the A-D path (the depth direction), FE simulation residual stresses for the UIT-treated model were analyzed and compared with those for the as-welded model. **Figures 10** and **11** depict residual stresses of butt joint and T-joint, respectively. As shown in **Figure 10**, before the UIT, the transverse, longitudinal and through-thickness residual stresses of butt weld joint remained stable along the A-D path, with the average values of 189, 267 and 9 MPa. After the UIT, near the upper impacting surface of butt weld joint, the transverse, longitudinal and through-thickness residual stresses changed into compressive stresses with peak values of −150, −355 and −75 MPa. As for the T-joint, before the UIT, high tensile stresses which were close to the yield strength of the base metal appeared near the upper surface of the as-welded joint. The maximum values of the transverse, longitudinal and through-thickness residual stresses were 364, 372 and 151 MPa. Like the butt joint, after the UIT, the transverse, longitudinal and through-thickness residual stresses of T-joint also transformed into the compressive stresses. The peak values of compressive stresses in the transverse direction, the longitudinal direction and the through-thickness direction were −255, −320 and −70 MPa, respectively. It was noteworthy that the maximum compressive stresses in the longitudinal direction for both butt joint and T-joint were relatively higher than the compressive limit of 304L steel, which implied cold working by the UIT induced plastic deformation of the weld joint. The similar level of compressive residual stresses higher than the material's yield limit was also obtained and reported by previous studies [11, 28, 32].

It was also found that the influence of the UIT decreased with depth. For the butt joint, the depth of compressive stresses in three directions was around 2 mm. Similarly, as for the T-joint, the effective depth of compressive layer in the transverse, longitudinal and through thickness directions introduced by the UIT were 2.5, 2.3 and 3.1 mm, respectively. The depths of compressive residual stresses by UIT were similar with the results of previous studies [33].

http://dx.doi.org/10.5772/intechopen.72394

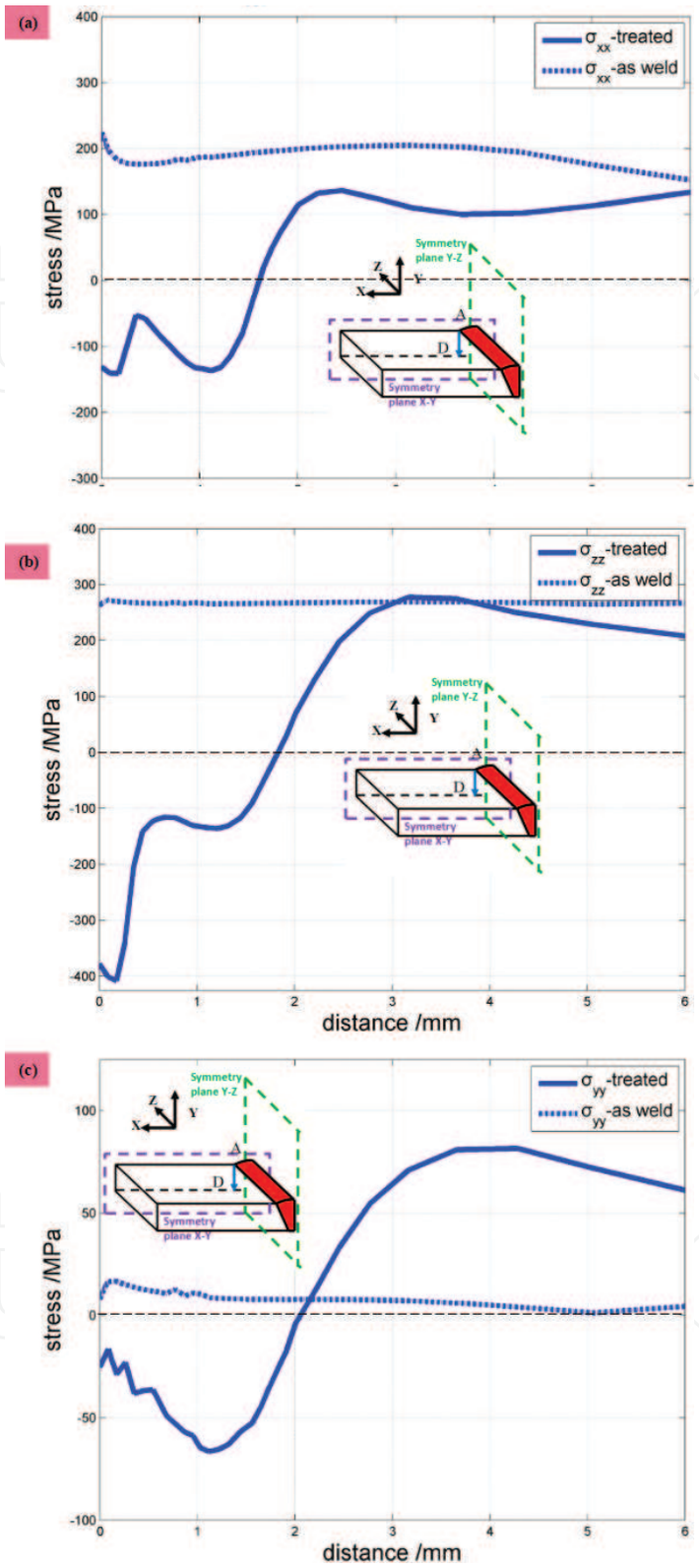

Figure 10. Transverse (a), longitudinal (b) and through-thickness (c) residual stress distributions along A-D path in as-welded and UIT-treated butt joints.

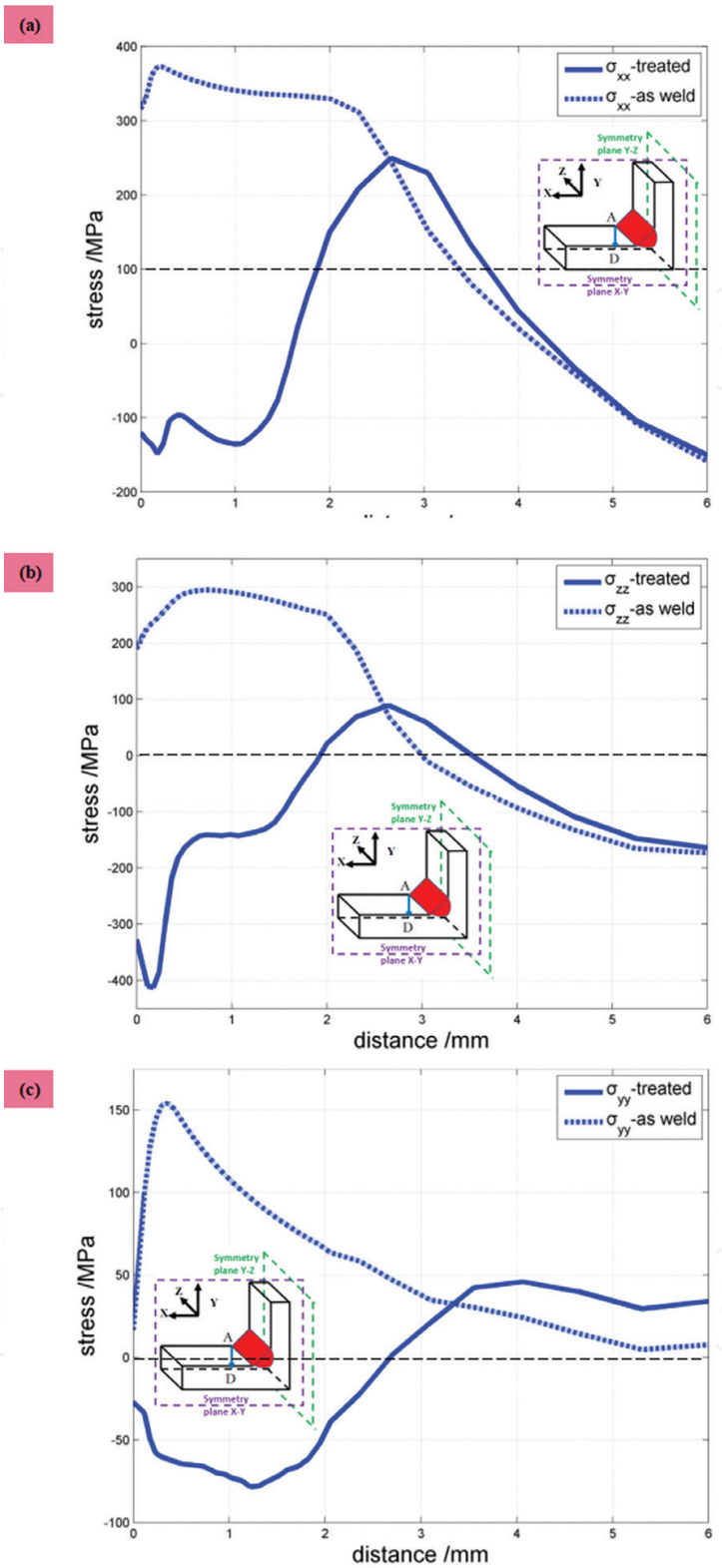

Figure 11. Transverse (a), longitudinal (b) and through-thickness (c) residual stress distributions along A-D path in as-welded and UIT-treated T-joints.

http://dx.doi.org/10.5772/intechopen.72394

The FE residual stress results in UIT-treated weld joint demonstrated that the UIT introduced compressive residual stress layer with various depth, which brought beneficial effect on fatigue strength of the material [7, 33–38].

4. Conclusions

This study focuses on evaluating effects of the UIT on the residual stresses of 304L butt and T-joints. FEA method was used to simulate both the welding and the UIT processes. To validate the prediction accuracy of the welding model, experimental data were compared with the simulated ones. Based on the results, the following conclusions can be drawn:

1. Both the simulation and the experimental results indicated that residual stresses reached their maximum values near the weld zone, then dropped with the increasing distance from the weld zone and finally stabilized the zero value.
2. The simulation results are in good agreement with the experimental results along the A-B path, confirming the welding model accuracy
3. The UIT introduces a compressive residual stress layer with depth between 2 and 3 mm near the impacting surface of weld joint. The effect of the UIT decreased with depth.

Author details

Lanqing Tang[1], Ayhan Ince[1,2]* and Jing Zheng[1]

*Address all correspondence to: aince@purdue.edu

1 Purdue Polytechnic Institute, Purdue University, West Lafayette, IN, USA

2 Department of Mechanical, Industrial and Aerospace Engineering, Concordia University, Montreal, Quebec, Canada

References

[1] Teng TL, Fung CP, Chang PH, Yang WC. Analysis of residual stresses and distortions in T-joint fillet welds. International Journal of Pressure Vessels and Piping. 2001;**78**:523-538. DOI: 10.1016/S0308-0161(01)00074-6

[2] Weich I, Thomas U, Thomas N, Dilger K, Chalandar HE. Fatigue behavior of welded high-strength steels after high frequency mechanical post-weld treatments. Weld World. 2009;**53**:R322-R332. DOI: 10.1007/BF03263475

[3] Abid M, Siddique M. Numerical simulation to study the effect of tack welds and root gap on welding deformations and residual stresses of a pipe-flange joint. International Journal of Pressure Vessels and Piping. 2005;**82**(11):860-871

[4] Chang KH, Lee CH. Finite element analysis of the residual stresses in T-joint fillet welds made of similar and dissimilar steels. International Journal of Advanced Manufacturing Technology. 2009;**41**:250-258

[5] Ferro P. The local strain energy density approach applied to pre-stressed components subjected to cyclic load. Fatigue and Fracture of Engineering Materials and Structures. 2014;**37**(11):1268-1280. DOI: 10.1111/ffe.12211

[6] Ferro P, Berto F, James NM. Asymptotic residual stress distribution induced by multi-pass welding processes. International Journal of Fatigue. 2017;**101**:421-429

[7] Rakesh R, Ghahremani K, Walbridge S, Ince A. Testing and fracture mechanics analysis of strength effects on the fatigue behavior of HFMI-treated welds. Weld World. 2016;**60**:987-999. DOI: 10.1007/s40194-016-0354-4

[8] Marquis GB, Mikkola E, Yildirim HC, Barsoum Z. Fatigue strength improvement of steel structures by high-frequency mechanical impact: Proposed fatigue assessment guidelines. Welding in the World. 2013;**57**:803-822. DOI: 10.1007/s40194-016-0354

[9] Statnikov ES. Applications of operational ultrasonic impact treatment (UIT) technologies in production of welded joints. Welding in the World. 2000;**44**:11-21

[10] Deng D, Murakawa H. Numerical simulation of temperature field and residual stress in multi-pass welds in stainless steel pipe and comparison with experimental measurements. Computational Materials Science. 2006;**37**:269-277. DOI: 10.1016/j.commatsci.2005.07.007

[11] Turski M, Clitheroe S, Evans AD, Rodopoulos C, Hughes DJ, Withers PJ. Engineering the residual stress state and microstructure of stainless steel with mechanical surface treatments. Applied Physics A. 2010;**99**:549-556. DOI: 10.1007/s00339-010-5672-6

[12] Liu Q, Ge DJ, Chen FG, Zou JS. Residual stress variation in a thick welded joint after ultrasonic impact treatment. Science and Technology of Welding and Joining. 2016;**21**:634-631. DOI: 10.1080/13621718.2016.1149932

[13] Foehrenbach J, Hardenecke V, Farajian M. High frequency mechanical impact treatment (HFMI) for the fatigue improvement: Numerical and experimental investigations to describe the condition in the surface layer. Welding in the World. 2016;**60**:749-755. DOI: 10.1007/s40194-016-0338-4

[14] Dekhtyar AI, Mordyuk BN, Savvakin DG, Bondarchuk VI, Moiseeva IV, Khripta NI. Enhanced fatigue behavior of powder metallurgy Ti–6Al–4V alloy by applying ultrasonic impact treatment. Materials Science and Engineering: A. 2015;**641**:348-359. DOI: 10.1016/j.msea.2015.06.072

[15] Guo CB, Wang ZJ, Wang DP. Numerical analysis of the residual stress in ultrasonic impact treatment process with single-impact and two-impact models. Applied Surface Science. 2015;**347**:596-601. DOI: 10.1016/j.apsusc.2015.04.128

[16] Mordyuka BN, Iefimovb MO, Prokopenkoa GI, Goluba TV, Danylenkob MI. Structure, microhardness and damping characteristics of Al matrix composite reinforced with AlCuFe or Ti using ultrasonic impact peening. Surface and Coatings Technology. 2010;**204**:1590-1598. DOI: 10.1016/j.surfcoat.2009.10.009

[17] Muránskya O, Hamelina CJ, Smithb MC, Bendeicha PJ, Edwardsa L. The effect of plasticity theory on predicted residual stress fields in numerical weld analyses. Computational Materials Science. 2012;**154**:125-134. DOI: 10.1016/j.commatsci.2011.10.026

[18] Le Pécheura A, Curtitb F, Clavela M, Stephanb JM, Reya C, Bomparda P. Thermomechanical FE model with memory effect for 304L austenitic stainless steel presenting microstructure gradient. International Journal of Fatigue. 2012;**45**:106-115. DOI: 10.1016/j.ijfatigue.2012.05.016

[19] Mahmoudi AH, Pezeshki-Najafabadi SM, Badnava H. Parameter determination of Chaboche kinematic hardening model using a multi objective Genetic Algorithm. Computational Materials Science. 2011;**50**:1114-1122. DOI: 10.1016/j.commatsci.2010.11.010

[20] Chaboche JL. A review of some plasticity and viscoplasticity constitutive theories. International Journal of Plasticity. 2008;**24**:1642-1693. DOI: 10.1016/j.ijplas.2008.03.009

[21] Yang XJ, Zhou JX, Ling X. Study on plastic damage of AISI 304 stainless steel induced by ultrasonic impact treatment. Materials & Design. 2012;**36**:477-481. DOI: 10.1016/j.matdes.2011.11.023

[22] Yuan KL. Modelling of ultrasonic impact treatment (UIT) of welded joints and its effect on fatigue strength. Frattura ed Integrità Strutturale. 2015;**34**:476-486. DOI: 10.3221/IGF-ESIS.34.53

[23] Zheng H, Liu DF, Lee CF, Tham LG. Displacement-controlled method and its applications to material non-linearity. International Journal for Numerical and Analytical Methods in Geomechanics. 2005;**29**:209-226. DOI: 10.1002/nag.410

[24] Tang LQ, Li HF, Wang XX, Qian CF. Numerical simulation and experimental investigation of residual stress in 06Cr19Ni10 austenitic stainless steel weld joint with effects of strain-strengthening. Applied Mechanics and Materials. 2017;**853**:204-208. DOI: 10.4028/www.scientific.net/AMM.853.204

[25] Goldak J, Chakravarti A, Bibby M. A new finite element model for welding heat sources. Metallurgical Transactions B. 1984;**15**:299-305. DOI: 10.1007/BF02667333

[26] Zheng J, Ince A. Numerical modeling and simulation of welding residual stresses using finite element method. In: 8th International Conference on Physical and Numerical Simulation of Materials Processing; 2016; Seattle, Washington

[27] Liang W, Murakawa H, Deng D. Investigation of welding residual stress distribution in a thick-plate joint with an emphasis on the features near weld end-start. Materials & Design. 2015;**67**:303-312. DOI: 10.1016/j.matdes.2014.11.037

[28] Smith DJ, Garwood SJ. Influence of postweld heat treatment on the variation of residual stresses in 50 mm thick welded ferritic steel plates. International Journal of Pressure Vessels and Piping. 1992;**51**:241-256. DOI: 10.1016/0308-0161(92)90083-R

[29] Mitra A, Prasad NS, Ram GDJ. Estimation of residual stresses in an 800 mm thick steel submerged arc weldment. Journal of Materials Processing Technology. 2016;**229**:181-190. DOI: 10.1016/j.jmatprotec.2015.09.007

[30] Xu JJ, Zhu ZQ, Chen LG, Ni CZ. Temperature distribution and residual stresses during multipass narrow gap welding of thick plates. Materials Science and Technology. 2006;**22**:232-237. DOI: 10.1179/174328406X83897

[31] Ji SD, Fang HY, Liu XS, Meng QG. Influence of a welding sequence on the welding residual stress of a thick plate. Modelling & Simulation in Materials Science & Engineering. 2005;**13**:553-566. DOI: 10.1088/0965-0393/13/4/006

[32] Roy S, Fisher JW, Yen BT. Fatigue resistance of welded details enhanced by ultrasonic impact treatment (UIT). International Journal of Fatigue. 2003;**25**:1239-1247. DOI: 10.1016/S0142-1123(03)00151-8

[33] Yuan K, Sumi Y. Simulation of residual stress and fatigue strength of welded joints under the effects of ultrasonic impact treatment (UIT). International Journal of Fatigue. 2016;**92**:321-332. DOI: 10.1016/j.ijfatigue.2016.07.018

[34] Liu Y, Wang DP, Deng CY, Xia LQ, Huo LH, Wang LJ, Gong BM. Influence of re-ultrasonic impact treatment on fatigue behaviors of S690QL welded joints. International Journal of Fatigue. 2014;**66**:155-160. DOI: 10.1016/j.ijfatigue.2014.03.024

[35] Ghahremani K, Ranjan R, Walbridge S, Ince A. Fatigue strength improvement of aluminum and high strength steel welded structures using high frequency mechanical impact treatment. Procedia Engineering. 2015;**133**:465-476. DOI: 10.1016/j.proeng.2015.12.616

[36] Ince A. A novel technique for multiaxial fatigue modelling of ground vehicle notched components. International Journal of Vehicle Design. 2015;**67**:294-313. DOI: 10.1504/IJVD.2015.069486

[37] Ince A. A computational multiaxial model for stress-strain analysis of ground vehicle notched components. SAE International Journal of Engines. 2017;**10**:316-322. DOI: 10.4271/2017-01-0329

[38] Ince A, Bang A. Deviatoric Neuber method for stress and strain analysis at notches under multiaxial loadings. International Journal of Fatigue. 2017;**102**:229-240. DOI: 10.1016/j.ijfatigue.2017.05.007